Build Simul (2021) 14: 749–762
https://doi.org/10.1007/s12273-020-0690-6

Analysis of the factors influencing the airflow behavior in an impinging jet ventilation room

Xiufeng Yang[2], Xiao Ye[1,3], Bin Zuo[2], Ke Zhong[1] (✉), Yanming Kang[1] (✉)

1. School of Environmental Science and Engineering, Donghua University, Shanghai, 201620, China
2. School of Hydraulic, Energy and Power Engineering, Yangzhou University, Yangzhou, 225127, China
3. School of Mechanical and Automobile Engineering, Shanghai University of Engineering Science, Shanghai 201620, China

Abstract

A validated CFD model is employed to predict the airflow behavior in an impinging jet ventilation (IJV) room with cool, isothermal or warm jets. By using the numerical results, the influences of jet discharge height, supply grille shape and room height on the jet flow behavior as well as the draught discomfort are analyzed for IJV operating in heating scenarios. The results indicate that the warm supply jet of IJV rises upward to the ceiling after spreading along the floor for a certain distance due to thermal buoyancy, resulting in a limited dispersion area, while the cool and isothermal jets of IJV always spread along the whole floor. When IJV is used for space heating, the lower the jet discharge height, the farther the supply air spreads along the floor, and the supply grille shape and room height almost have no effect on the air dispersion area. The results also show that the energy-efficient advantage of IJV in its heating mode compared to the mixing ventilation (MV) system is more remarkable in higher rooms. Moreover, there is a risk of draught discomfort in IJV heating rooms and it is recommended to wear socks to avoid this discomfort.

Keywords

impinging jet ventilation,
heating scenario,
airflow behavior,
draught discomfort

Article History

Received: 01 July 2019
Revised: 06 July 2020
Accepted: 16 July 2020

1 Introduction

Although the displacement ventilation (DV) has been widely used for building ventilation in the past decades due to its high ventilation efficiency and high energy efficiency, it can only be used for cooling and is not suitable for heating (Karimipanah and Awbi 2002; Awbi 2003; Ye et al. 2016). To overcome this problem, a new ventilation system impinging jet has been developed and studied by Awbi (2003), Karimipanah and Awbi (2002), Varodompun (2008) and some others (e.g. Chen et al. 2012, 2013a, 2013b; Chen 2014; Chen et al. 2015; Ye et al. 2016, 2017, 2018).

In an impinging jet ventilation (IJV) room, as has been reviewed by Ye et al. (2017, 2018) recently, a high momentum air jet is discharged downwards at low room level, strikes the floor and spreads over a large area, causing the jet momentum to recede yet allowing the jet to reach long distances (Karimipanah and Awbi 2002; Ye et al. 2017). This scenario of air distribution has advantages over both DV and mixing ventilation (MV).

One advantage of IJV is that it produces a clean air zone in the lower part of the occupied zone and exhibits higher air-exchange effectiveness than the MV system. Another advantage is that it can be used not only for room cooling but also for space heating, giving it greater working flexibility than the DV system. Moreover, the warm supply jet of IJV is directly delivered to the occupied zone unlike the MV system which cannot distribute the warm air into the lower parts of room effectively. Consequently, the IJV system has the potential to be an alternative to the DV and MV systems (Awbi 2003; Karimipanah and Awbi 2002).

Although the biggest advantage of IJV is that it can meet the requirement not only of room heating but also of room cooling efficiently, most of the existing studies focus on the cooling or isothermal scenario. Only a few studies have been done to evaluate the ventilation performance of IJV operating in heating mode up to now. For example, Gauntner et al. (1970) reviewed the flow field of a single impinging jet and presented the methods for determining the pressure and velocity profiles in the IJV room. Beltaos

E-mail: zhongkeyx@dhu.edu.cn (Ke Zhong); ymkang@dhu.edu.cn (Yanming Kang)

List of symbols

c_μ	empirical constant specified in the turbulence model
C_p	specific heat capacity of air (kJ/(kg·K))
d_h	hydraulic diameter of the jet discharged section
g_i	the ith component of the gravitational acceleration
h	jet discharge height (m)
H	room height (m)
l	length scale (m)
k	turbulent kinetic energy (J/kg)
k_{in}	turbulent kinetic energy at the inlet (J/kg)
$\overline{P}$	mean pressure (Pa)
PD	percentage dissatisfied (%)
Pr_t	turbulent Prandtl number (dimensionless)
Re_{dh}	Reynolds number at the inlet (dimensionless)
S	area of the supply grille (m^2)
T	air temperature (°C)
$\overline{T}$	mean temperature (°C)
T_{cl}	mean skin temperature (°C)
T_e	exhaust temperature (°C)
T_r	reference air temperature (°C)
T_s	supply temperature (°C)
T_u	turbulence intensity (dimensionless)
ΔT	temperature difference between the jet and indoor air (°C)
u	air velocity (m/s)
$\overline{u}$	mean air velocity (m/s)
u'	fluctuating component of air velocity (m/s)
u_s	supply velocity of the jet (m/s)
V	dimensionless air velocity
z	vertical location (m)
Z	dimensionless vertical location
β	thermal expansion coefficient of air (K^{-1})
δ_{ij}	Kronecker delta
ε_{in}	turbulent dissipation rate at the inlet (m^2/s^3)
λ	air thermal conductivity (W/(m·K))
ρ	air density (kg/m^3)
ρ_r	reference air density related to T_r (kg/m^3)
ν	kinematic viscosity of air (m^2/s)
ν_t	turbulent eddy viscosity (m^2/s)
θ	dimensionless air temperature

Subscripts

i and j	three dimensions in the Cartesian coordinate system

and Rajaratnam (1973, 1974, 1977) suggested that the flow field of an impinging jet can be divided into three regions including free jet region, impingement region and wall jet region, and described the flow features in the three regions. Gutmark et al. (1978) examined experimentally the turbulent structure on the center line of a two-dimensional isothermal impinging jet and pointed out that the impingement of the jet is not affected by the presence of the plate and the turbulent properties of the jet in a certain range of parameters. Cooper et al. (1993) experimentally investigated the velocity field characteristics of a turbulent circular impinging jet and analyzed the axial velocity decay, the rate of jet growth and the radial velocity distribution. Knowles and Myszko (1998) studied the effect of nozzle height on the thickness of a wall-jet with fixed nozzle pressure ratio in an IJV room during the cooling season. Karimipanah and Awbi (2002) presented the experimental data on a cool impinging jet and derived a non-dimensional expression for the decay of maximum velocity over the floor to evaluate the performance of an IJV system and compare it with a DV system. Rajaratnam and Pani (1974) and Zhao et al. (2004) discussed the impact of nozzle geometry on the development of a three-dimensional wall jet. The non-dimensional velocity profiles were found similar in all cases at a distance 10 times greater than the nozzle height. Guerra et al. (2005) measured the velocity and temperature fields near a wall in an IJV room for the cases of constant nozzle-to-plate spacing and Reynolds number. Xu and Hangan (2008) discussed the effects of Reynolds number, nozzle shape and the confinement of surrounding boundaries on the flow field characteristics in a cooling room equipped with IJV. Chen et al. (2013b) investigated the influences of the discharge height, shape of air supply device and supply parameters on the airflow and thermal behavior in an office with the IJV system in cooling mode. Yao et al. (2015) conducted an experimental investigation of the flow characteristics of an isothermal impinging jet in a closed cabin and analyzed the multi-scale structure of the jet impingement. Taghinia et al. (2015) evaluates the performance of two turbulence models in predicting the indoor airflow for three ventilation scenarios including the IJV in isothermal mode.

In addition to the above airflow behavior, studies about the thermal comfort, indoor air quality and energy consumption characteristics of IJV operating in cooling or isothermal mode have been done in the literature (e.g. Varodompun 2008; Chen et al. 2012, 2013a, 2013b; Chen et al. 2015). Varodompun (2008) studied the indoor air quality and ventilation effectiveness of the IJV and DV systems in different space volumes, respectively. Chen et al. (2012, 2013a, 2015) experimentally and numerically studied the velocity and temperature fields in IJV rooms during the cooling season. Zuo et al. (2015) studied the particle

resuspension caused by supply conditions in a room with the IJV system in cooling mode. It was found that when the supply velocity is less than 3 m/s, particle resuspension does not occur in the room. Haghshenaskashani et al. (2018) presents a Taguchi method-based CFD study to analyze the influence of operating conditions of the IJV system in cooling mode on the overall performance of thermal comfort, indoor air quality and system energy performance. As for the heating cases, Ye et al. (2016, 2017, 2018) studied the distribution patterns of indoor thermal environment, energy consumption and the warm air spreading distance.

It should be noted that there is no study referring to the comparisons of the airflow pattern and the jet velocity decay after the jet hits the floor between the isothermal, cooling and heating scenarios. In particular, there is a lack of research on the influences of supply grille shape, jet discharge height and room height on the airflow pattern in IJV heating rooms, though these effects are different from that in a cooling or isothermal IJV room due to the fact that the direction of the buoyancy force acting on the cool and warm air is opposite. In the present study, a CFD technique is used to investigate the difference of the flow behavior between the cool, isothermal and warm jets on one hand. On the other hand, the influences of some factors including jet supply parameters, supply grille geometry and room height on the indoor airflow behavior are discussed in IJV heating rooms. Also, the effect of supply velocity on the draught discomfort induced by IJV used for room heating is analyzed in detail.

2 Numerical simulation

2.1 Physical model

When IJV is used in a large space, the effect of room confinement is ignored for most supply jets. Chen et al. (2012) indicated that the confinement effect mainly influences the region far from the inlet wall. The modeling space should therefore be large enough to simulate the flow pattern of the impinging jet when spreading along the floor without confinement.

Based on the study by Varodompun (2008), the terminal configuration of the IJV system is important and it is possible to integrate the terminals with architectural elements, such as walls and columns. For example, IJV terminals might be integrated with columns on one side or on both sides, or the terminal may encircle the column. In this study, the IJV terminal surrounds a column located at the center of a room.

To perform the simulations of the airflow pattern and the temperature distribution in a large space, as shown in Figure 1, it is not necessary to assume the whole space as the region for analysis due to the symmetry of the geometrical configuration of the space. For the sake of simplifying the numerical simulation, it is assumed that the modeled room and its adjacent rooms are at the same temperature, the floor of the modeled room are considered to be adiabatic, and the four surrounding "walls" of the region for analysis are symmetric planes of the airflow (see the blue lines in Figure 1).

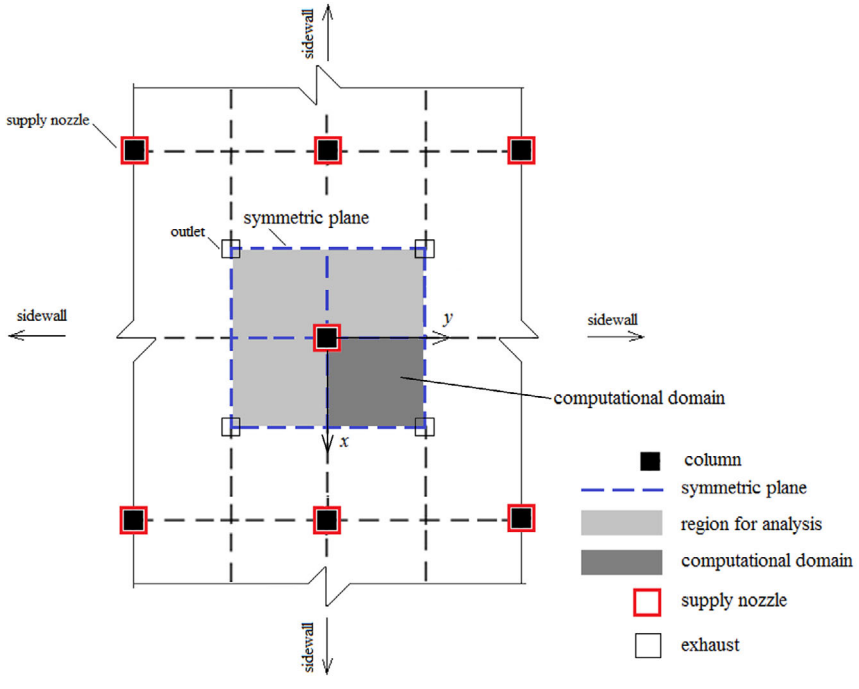

Fig. 1 Schematic of the computational domain of the large space in this study

So the physical model used in this study is simplified and shown in Figure 2. The space under consideration has a dimension of 18.0 m (x) × 18.0 m (y) × H (z) (H = 6.0, 9.0, 18.0 or 24.0 m), see Figure 2(a), which can be regarded as an IJV room without confinement effect. The air is supplied through a duct and discharged at different heights downwards the floor, so the supply velocity direction is along the negative z-axis. The nozzle surrounds the column with a cross section of 0.6 m × 0.6 m in the middle of the room, the area (S) of the supply grille is assumed to be 0.13 m^2 (Figure 2(b)), and the discharge heights of the jet (h) are 0.6, 0.9 and 1.2 m. Exhaust air is extracted from four outlets (0.2 m × 0.2 m) located on the ceiling, and symmetry plane boundary conditions are used at two planes (i.e., Planes A and B) bisecting the building blocks along x and y directions, as shown in Figure 2(a). Thus, the computational domain can be reduced to one-quarter of the space under consideration.

To further simplify the physical model, internal heat sources are ignored and the heating load is assumed to be generated only by the heat transfer through the ceiling when the IJV is used for heating. For the case of a cool jet, the cooling load is considered to be caused by the heat transfer through the ceiling and two heat sources on the floor, where each source consists of two human simulators standing together (see Figure 2(c)). Each simulator has a dimension of 1.0 m × 0.5 m × 1.8 m corresponding to standing people, and the surface temperature is set at 30 °C.

Since the energy efficiency of IJV might be slightly affected by the space height, the mean temperature of the occupied zone (below the height of 1.8 m in a space) might be different for different ceiling heights despite the same ceiling temperature and the same supply parameter. For comparison, ceiling temperatures are determined after trial calculations to make the mean temperatures of the occupied zone be about 20 °C and 25 °C for the heating and cooling cases, respectively. The floor and the surrounding walls are considered to be adiabatic on the premise that the modeled room and its adjacent rooms are at the same temperature.

The following factors are considered: the temperature difference between the jet and indoor air (ΔT), the supply velocity of jet (u_s), the discharge height of jet (h), the supply grille shape and the room height (H), to investigate their influences on the airflow behavior in IJV rooms. As for the influence of the supply grille shape, three types of grille, i.e., square, diamond and circular grilles, are investigated, see Figure 2(d). The cross-section areas of columns in the three cases are equal to that of the column shown in Figure 2(b), and all the grille areas for the three cases are equal to 0.36 m^2 ± 0.01.

2.2 Governing equations and turbulence model

The airflow field inside the IJV room can be described by the conservation laws of mass, momentum and energy, and the flow is assumed to be three-dimensional, steady-state, incompressible and turbulent flow. The physical properties of the air are assumed constant, except that the air density is assumed to follow the Boussinesq approximation. The time-averaged conservation equations are as follows (Chen et al. 2012; Ye et al. 2017):

$$\frac{\partial \overline{u}_i}{\partial x_i} = 0 \tag{1}$$

$$\overline{u}_j \frac{\partial (\overline{u}_i)}{\partial x_j} = -\frac{1}{\rho}\frac{\partial \overline{P}}{\partial x_i} + \frac{\partial}{\partial x_j}(\nu \frac{\partial \overline{u}_i}{\partial x_j} - \overline{u_i' u_j'}) + g_i \beta (\overline{T} - T_r) \tag{2}$$

$$\overline{u}_j \frac{\partial (C_p \overline{T})}{\partial x_j} = \frac{\partial}{\partial x_j}\left(\frac{\lambda}{\rho}\frac{\partial \overline{T}}{\partial x_j}\right) - \frac{\partial}{\partial x_j}(C_p \overline{u_j' T'}) \tag{3}$$

where ρ and λ are the air density and thermal conductivity, respectively, ν is the kinematic viscosity, C_p is the specific heat capacity of air, and T_r is the reference temperature (T_r = 20 °C for heating mode and 25 °C for cooling mode). The subscripts, i and j = 1, 2, 3, are the three dimensions in the Cartesian coordinate system (i.e., x, y and z), and $\overline{u}_i$ and g_i are the ith components of the averaged velocity and the

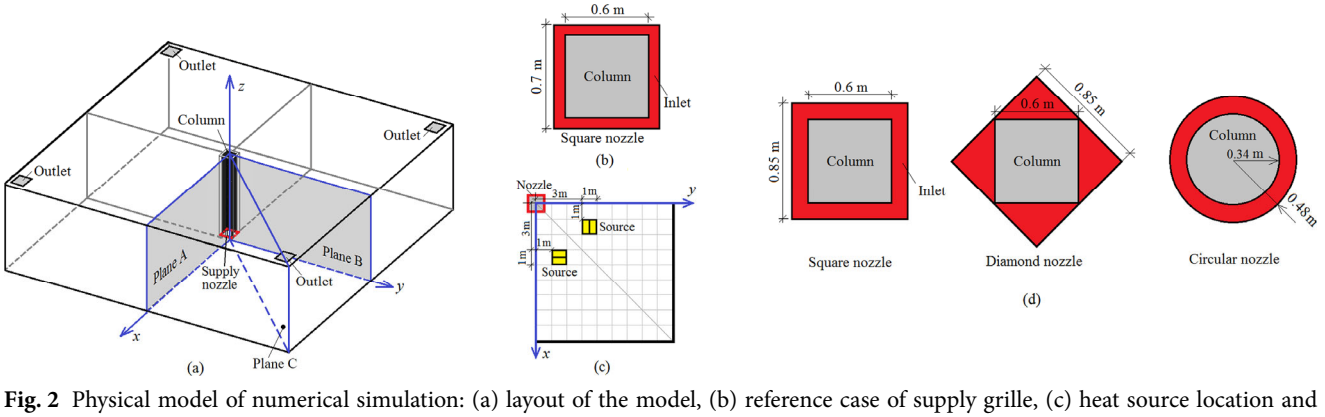

Fig. 2 Physical model of numerical simulation: (a) layout of the model, (b) reference case of supply grille, (c) heat source location and (d) supply grille geometries for comparison

gravitational acceleration, respectively. The terms $-\overline{u_i'u_j'}$ and $-\overline{u_j'T'}$ are the unknown Reynolds stresses and turbulent heat fluxes, respectively. $\overline{T}$ and $\overline{P}$ are the mean temperature and pressure, respectively.

The thermal expansion coefficient of air, β, is defined as:

$$\beta = -\frac{1}{\rho_r}\cdot\frac{\partial\rho}{\partial T} \approx -\frac{\rho-\rho_r}{\rho_r(\overline{T}-T_r)} \tag{4}$$

where ρ_r is the reference density related to T_r. In the present study, the Boussinesq approximation applies since the difference between the supply and the indoor air is around 10 °C (cooling mode) and 15 °C (heating mode), respectively. Thus β is assumed to be about 3.32×10^{-3}.

The terms $-\overline{u_i'u_j'}$ and $-\overline{u_j'T'}$ contained in Eqs. (2) and (3) can be approximately modeled by using the Boussinesq hypothesis. The Reynolds stress tensor is associated with mean velocity gradient through eddy viscosity (Chen et al. 2012):

$$-\overline{u_i'u_j'} = \nu_t\left(\frac{\partial\overline{u_i}}{\partial x_j}+\frac{\partial\overline{u_j}}{\partial x_i}\right)-\frac{2}{3}\left(k+\nu_t\frac{\partial\overline{u_i}}{\partial x_i}\right)\delta_{ij} \tag{5}$$

and the turbulent heat fluxes are expressed as:

$$-\overline{u_j'T'} = \frac{\nu_t}{Pr_t}\frac{\partial\overline{T}}{\partial x_j} \tag{6}$$

where ν_t is the turbulent eddy viscosity, k is the turbulent kinetic energy which is determined through $k=\overline{u_i'u_i'}/2$, δ_{ij} is the Kronecker delta ($i=j$, $\delta_{ij}=1$; $i\neq j$, $\delta_{ij}=0$), and Pr_t is turbulent Prandtl number, and $Pr_t=0.85$.

Chen et al. (2012) validated two turbulence models of RNG k-ε and SST k-ω with experimental findings. The results indicate that both of the turbulence models are capable of capturing the main flow feature of the isothermal impinging jet. Chen (1995) discussed five turbulence models for indoor air flow computations and pointed out that both the RNG k-ε turbulence model and standard k-ε turbulence model can provide steady results, and the former performs better predictions for flow separation, streamline curvature and flow stagnation. Because of the robustness and relatively low computational cost, the RNG k-ε turbulence model was employed in the current investigation to achieve closure in the governing equations. Details of these advantages can be found in Chen et al. (2012) and Ye et al. (2016).

2.3 Numerical details and boundary condition

The finite-volume solver (ANSYS Fluent 6.3.26) is used to numerically simulate the flow field in an impinging jet ventilated room. The governing equations are solved with the segregated scheme and the pressure-velocity coupling is controlled by the SIMPLE algorithm. The non-linear terms and the viscous terms of the governing equations are discretized using the second-order upwind scheme and the second-order central scheme, respectively, and the pressure is discretized with a standard scheme. The residuals of continuity, momentum, turbulent kinetic energy and its dissipation rate have to reach 10^{-3} in magnitude for convergence, while the residual of energy has to reach 10^{-6}.

A velocity inlet boundary condition is set at the inlet of the computational domain, and inlet values of the turbulent kinetic energy (k_{in}) and its dissipation rate (ε_{in}) profiles are specified as follows:

$$k_{in} = 1.5(u_s T_u)^2 \tag{7a}$$

$$\varepsilon_{in} = c_\mu^{3/4}k_{in}^{3/2}/l \tag{7b}$$

where c_μ is the empirical constant specified in the turbulence model with an approximate value of 0.0845. The length scale, l, is defined as $l=0.07d_h$, and d_h is the hydraulic diameter at the jet discharged section (Chen et al. 2013a). T_u is the turbulence intensity determined by:

$$T_u = 0.16(Re_{dh})^{-1/8} \tag{8}$$

where Re_{dh} is the Reynolds number at the inlet defined by $Re_{dh}=l\cdot u_s/\nu_{in}$, and ν_{in} is the kinematic viscosity of the supply air.

For the outlets of the domain, outflow boundary conditions are assumed and all the solid surfaces are specified as no-slip walls. Meanwhile, the standard wall function is employed to model the turbulence in the vicinity of the walls with low Reynolds number (Launder and Spalding 1974). A total of 18 case studies are simulated, and boundary conditions and other parameters are listed in Table 1, where T_{in} is the mean indoor temperature and $T_{ceiling}$ is the averaged temperature of the ceiling surface.

2.4 Grid independency

To cover the whole computational domain efficiently, a non-uniform grid distribution is used, i.e., finer mesh is constructed close to the inlet, outlet and walls as well as the regions expected to have steep velocity gradients.

A grid independence study is performed by testing and adjusting the cell sizes. If the differences in the calculated velocity and temperature for different grid densities are less than 10^{-3} m/s and 10^{-3} °C, respectively, grid independence is considered reached, with the details of this contention found elsewhere (Ye et al. 2016). The final mesh sizes range from 0.005 m at the inlet to 0.15 m in open spaces. Grids

Table 1 Boundary conditions and other parameters of case studies

Case	T_s (°C)	T_{in} (°C)	ΔT (°C)	u_s (m/s)	h (m)	S (m^2)	H (m)	$T_{ceiling}$ (°C)	Airflow rate (m^3/h)	Re_{dh}	Supply grille shape	Note
1	18	24.8	~ −7	2.0	0.6	0.13	9.0	31.5	936	16348	Square	Section 3.1
2	20	25.0	−5	2.0	0.6	0.13	9.0	29.8	936	16034		
3	22	25.1	−3	2.0	0.6	0.13	9.0	28.0	936	15750		
4	—	—	0	2.0	0.6	0.13	9.0	20.0	936	16034		
5	23	20.1	3	2.0	0.6	0.13	9.0	17.2	936	15554		
6	25	19.9	5	2.0	0.6	0.13	9.0	15.1	936	15261		
7	27	19.8	~ 7	2.0	0.6	0.13	9.0	13.1	936	14974		
8	25	20.0	5	1.5	0.6	0.13	6.0	16.4	702	11446		Section 3.2.1
9	25	19.9	5	1.5	0.9	0.13	6.0	16.3	702	11446		
10	25	20.1	5	1.5	1.2	0.13	6.0	16.5	702	11446		
11	25	20.0	5	1.5	0.6	0.36	6.0	10.0	1944	28614	Square	Section 3.2.2
12	25	19.9	5	1.5	0.6	0.36	6.0	9.9	1944	28614	Diamond	
13	25	19.7	~ 5	1.5	0.6	0.36	6.0	9.7	1944	32047	Circular	
14	23	20.1	3	1.5	0.6	0.13	6.0	17.5	702	11666	Square	Section 3.2.3
15	23	19.9	3	1.5	0.6	0.13	9.0	17.7	702	11666		
16	23	20.0	3	1.5	0.6	0.13	16.0	17.8	702	11666		
17	23	20.1	3	1.5	0.6	0.13	24.0	17.9	702	11666		
18	23	19.8	~ 3	1.0	0.6	0.13	9.0	18.4	468	7777		Section 3.3

with about 4,360,000 – 4,840,000 cells in total are created in the computation domain to achieve grid independence and reasonable accuracy.

2.5 Numerical validation

To validate the numerical model when IJV is used for heating, the flow and temperature fields in a chamber with a warm impinging jet were investigated by both experimental measurement and numerical modeling. The physical model and boundary conditions of the numerical simulation are consistent with experiment. By comparing the predictions from different grids, the grid with 880,000 cells was considered sufficient for use in the physical model corresponding to the experiment to reach grid independence.

The experiments were performed in a test chamber with dimensions of 3.6 m × 3.0 m × 2.6 m ($L \times W \times H$), placed in a HVAC laboratory, see Figure 3(a). The chamber envelopes are made of color steel plates which are hollow and insulated with 7 cm thickness rock wool inside. The mean heat transfer coefficient of the envelopes is about 0.9 W/(m^2·°C). The chamber has one door with a sealing strip and has a 0.35 m × 0.35 m viewing window made of double glazing on the door. The percentage of the fresh air was regulated to 10% to maintain positive air pressure within the chamber during the experiments. Consequently, the heat loss due to air infiltration through envelope cracks, except for a large crack on the lower part of a side wall, can be ignored. To keep the air infiltration through the crack roughly constant, a fan outside the chamber was used to blow the air to the crack. Thus, the infiltration rate was kept at 0.003 m^3/s during the experiments, and the heating load was caused by the air infiltration and the heat transfer through envelopes.

Warm air was supplied through a duct of 0.2 m diameter and was discharged from the nozzle at h = 0.17 m, see Figure 3(b). The duct was placed at the middle of the east wall (x =0), and the outlet (0.2 m × 0.3 m) was located at the center of the ceiling. Fifty Type-K thermocouples, accurate to ± 0.1 °C, were used to measure the air temperature within the chamber. Air velocities were measured by hotwire anemometers (HD103T.0, Delta OHM Inc., Italy) with the accuracy of ± 2 fpm (± 0.01 m/s) or 2% in the range 0.05 – 5 m/s. There were four movable poles in the chamber, each with seven measuring points where the thermocouples and anemometers were instrumented. Along each pole, two additional thermocouples were located 0.02 m above the floor and below the ceiling, respectively. Twelve thermocouples were placed on the ceiling, surrounding walls, floor and the window to measure the surface temperatures of the chamber. The other two thermocouples were placed at the inlet and outlet. The arrangements of measuring poles and measuring points (denoted by "×" and "O", respectively) are shown in Figure 3(c). The computational model corresponding to

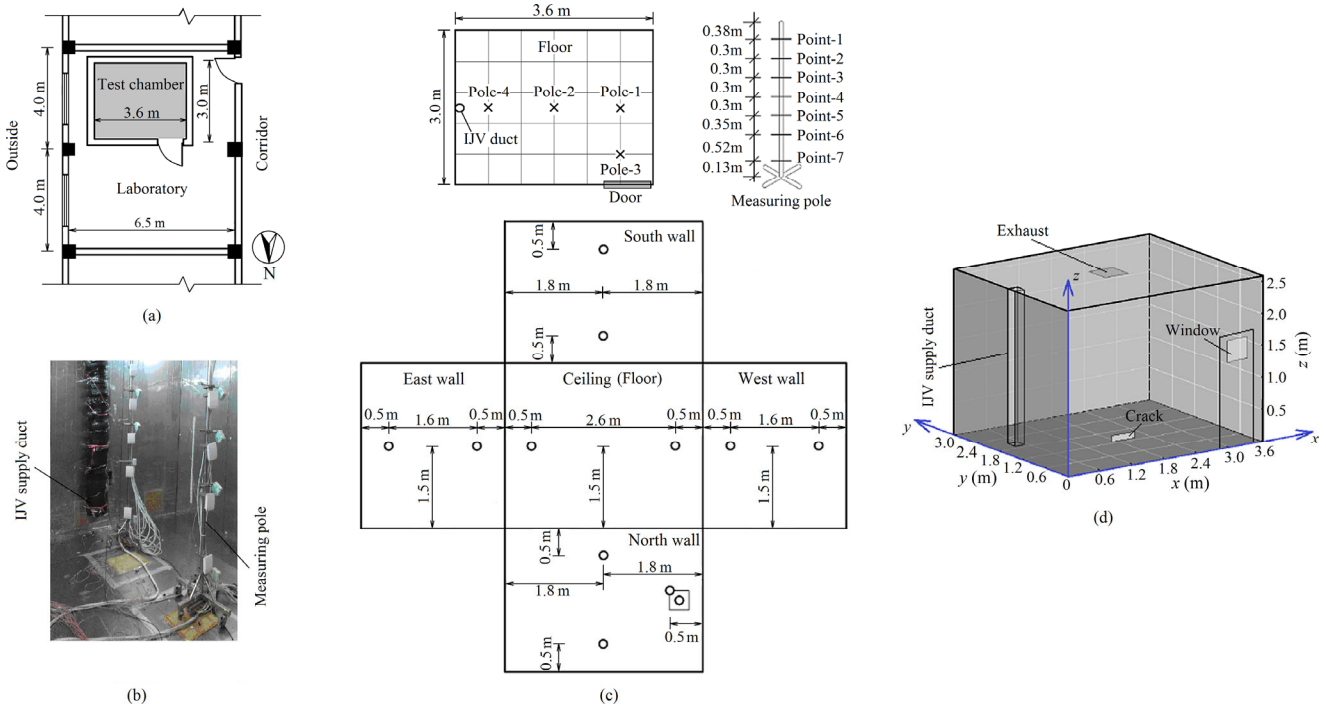

Fig. 3 Schematic view of the experimental system: (a) layout of the laboratory, (b) supply duct of the IJV system, (c) measuring poles and measuring points on the solid surfaces, (d) computational model

the test chamber is presented in Figure 3(d).

Air temperature outside the chamber can be adjusted to 10 ± 0.5 °C by an air-conditioning system. Measurements were conducted under steady-state conditions by stabilizing indoor thermal and fluid conditions for several hours before recording the data. The supply velocity and the temperature of the warm jet in the validation case were 1.2 m/s and 35.6 °C, respectively. The temperature of each wall was monitored at two points (see Figure 3(c)), and the measured averaged surface temperatures are listed in Table 2. In the validation case, the ceiling, the floor and all the walls were set as constant temperatures consistent with measurements.

Figure 4 presents the flow and temperature fields computed by CFD in the vertical middle plane through the nozzle. The warm air is shown to rise upwards after spreading along the floor for a short distance due to the high temperature difference (ΔT = 15.6 °C) between the supply and indoor air. Therefore, the air temperatures in the lower regions close to or far from the nozzle are higher or lower than those in other regions of the chamber, respectively.

Figure 5 and Figure 6 show the vertical temperature and velocity profiles, respectively, measured by experiments and computed by CFD simulation. The air temperature (T) is normalized by the supply temperature (T_s) and the exhaust temperature (T_e), i.e., $\theta = (T_s - T)/(T_s - T_e)$. The air velocity ($u$) and the vertical location (z), are respectively scaled by the supply velocity (u_s = 1.2 m/s) and the room height (H = 2.6 m), namely, $V = u/u_s$ and $Z = z/H$. Hence, Z = 0 and Z = 1 correspond to the heights of floor and ceiling, respectively. It was found that, during the experiments, the temperature in the chamber was steady with negligible fluctuation, so only the averaged values for the whole process of recording are given in Figure 5. While the velocities are shown by four groups of data (each data group was determined by the averaged value for one hour) because of the slight fluctuation of air velocity caused by the airflow turbulence, as indicated in Figure 6.

It can be observed from Figure 5 that the numerical results of the temperature are consistent with the test data in most regions of the room except those near the ground. The reason is that the temperature of the floor is set as the averaged value of the measurements at Pole-1 and Pole-4

Table 2 Measured temperature boundary conditions in the chamber with an IJV (°C)

		Inner surface						
Supply air	Indoor air	North wall	South wall	West wall	East wall	Floor	Window	Ceiling
35.6	20.0	19.6	19.4	19.8	19.4	16.0	18.2	20.1

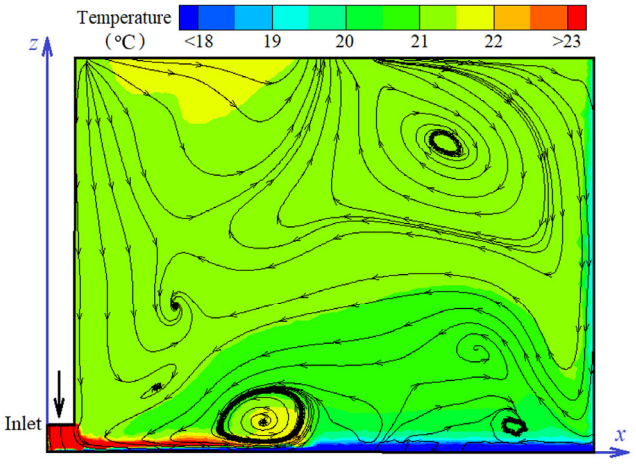

Fig. 4 Computed flow and temperature fields in the vertical middle plane of the chamber

when conducting numerical simulations. This approximation may result in some differences in the prediction of temperature in the region closes to the ground.

Figure 6 indicates that air velocities in most regions are lower than 0.1 m/s, except for the upper and lower regions near pole-4 and the region at the top of pole-2 which is close to the outlet. Due to the small magnitude of air velocity, the measurement errors of anemometers may exceed the accuracy to some extent. However, the velocity predictions from the RNG k-ε model exhibit reasonable agreement with the measured data.

The comparisons in Figures 4 and 5 indicate that the numerical model used in this study is appropriate for the simulation of both the temperature and flow fields in the IJV room.

3 Results and discussion

3.1 Difference of the flow pattern between cooling and heating jets

Figure 7 shows the streamlines of supply air in the vertical middle plane through the square grille (i.e., the vertical yz-plane at x = 0, Plane B in Figure 2) under three temperature differences (ΔT) of 0 °C, −3 °C and 3 °C between the supply air and indoor air, corresponding to isothermal, cool and warm jets, respectively. The room height (H), supply grille area (S), supply velocity (u_s), and jet discharge height (h) are identical for the three cases, i.e., H = 9.0 m, S =0.13 m^2, u_s = 2.0 m/s and h = 0.6 m.

As shown in Figure 7(a), an isothermal impinging jet with high momentum strikes the floor and distributes along the floor in the form of a very thin shear layer. When the airflow reaches the opposite wall, it continues to flow along the wall until it is held back by the ceiling and finally forms

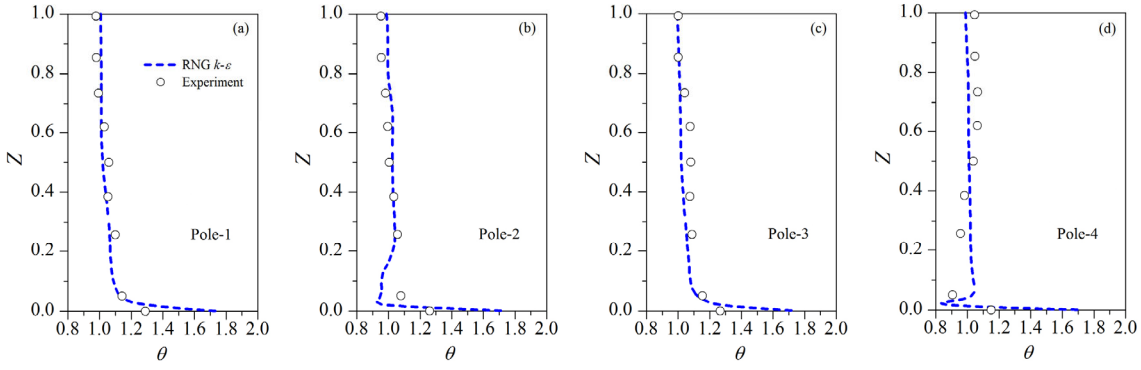

Fig. 5 Comparisons of the vertical temperature distributions between numerical results and test data

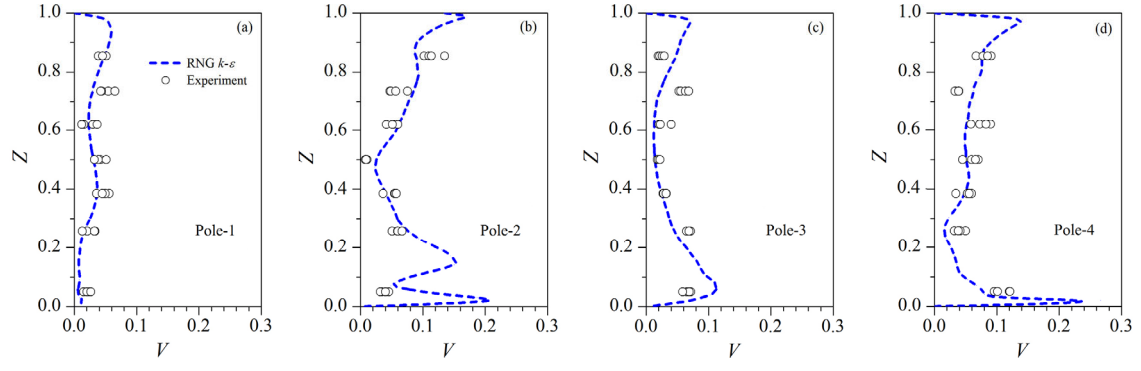

Fig. 6 Comparisons of the velocity profiles between numerical results and test data

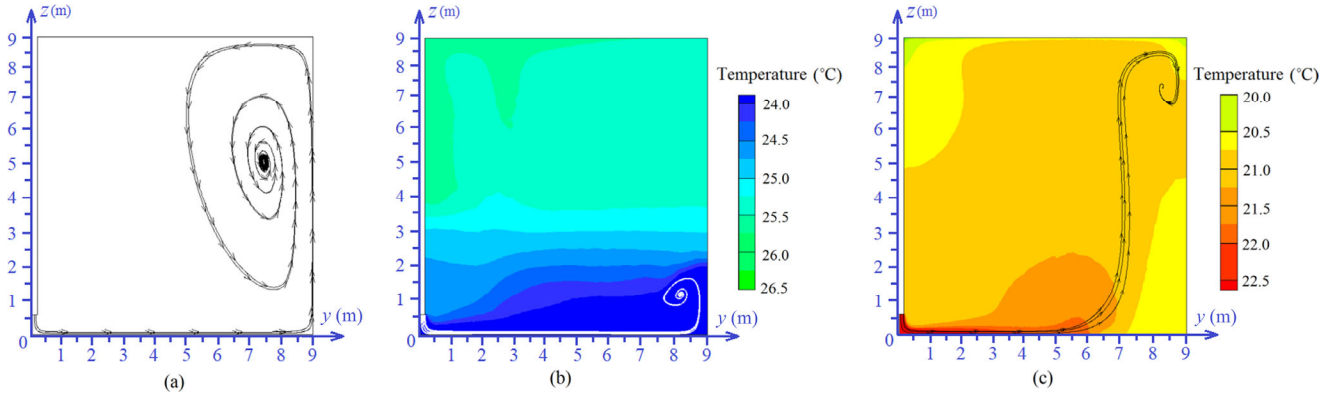

Fig. 7 Streamlines of supply air in Plane B (x = 0) in the case of: (a) isothermal jet, (b) cool jet and (c) warm jet

a large eddy below the ceiling.

Figure 7(b) shows the airflow pattern and temperature distribution in the room due to a cool jet. Since the buoyancy of cool air is downward, it has no impact on the supply air spreading along the floor. Unlike the isothermal jet, the cool air tends to leave the wall and flow downward to the lower part of the room because of the negative buoyancy, so the temperature distribution is similar to that of a DV room.

The airflow feature and temperature field of a warm jet are presented in Figure 7(c). It can be seen that the warm air deviates from the floor after flowing over it for a certain distance and gradually rises upward to the ceiling because it is affected by an upward buoyancy, so the dispersion area of the discharged warm air is limited, which is different from the flow pattern of a cool jet. Within the jet spreading region, higher temperature appears in the lower part, which would provide better thermal comfort and energy-efficiency.

The airflow pattern and temperature distribution in the vertical plane through the diagonal of the ground (i.e., Plane C in Figure 2) for the three cases above are presented in Figure 8. Since the supply nozzle and the outlet are both included in Plane C, the airflow behavior of IJV in Plane C may be more informative.

Figure 8(a) illustrates the airflow pattern of the isothermal impinging jet. The airflow rises upward after reaching the corner, and forms some small eddies because of the limited momentum after long-distance spreading along the diagonal of the ground. There are also some large eddies in Plane C, which means the well-mixed airflow pattern in the large area of the IJV room with isothermal jet.

Figure 8(b) shows the airflow behavior similar to that in Figure 7(b). The displacement airflow pattern develops and the temperature stratification is apparent. The laminar flow regime occurs near the outlet.

It can be found from Figure 8(c) that the warm air separates from the ground after spreading a certain distance and then rises upward, the spreading distance along the diagonal of the ground is smaller than those in other directions. The temperature distribution in Plane C is more uniform than those in other vertical planes such as Plane B because the jet spreading region along the diagonal of the ground is the smallest. The flow pattern near the outlet is the laminar flow similar to that in Figure 8(b).

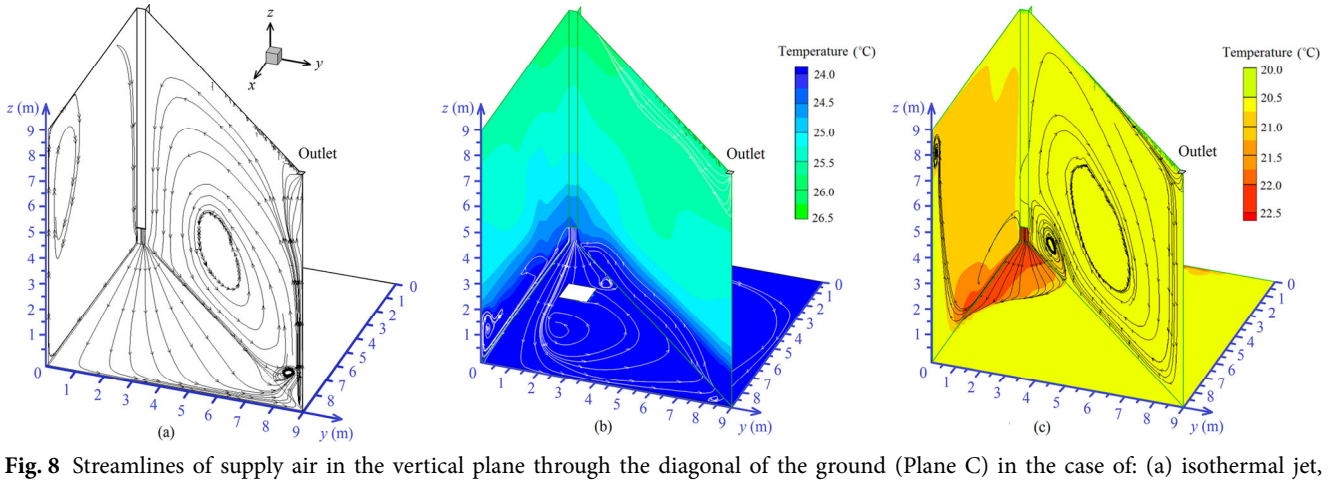

Fig. 8 Streamlines of supply air in the vertical plane through the diagonal of the ground (Plane C) in the case of: (a) isothermal jet, (b) cool jet and (c) warm jet

Overall, the airflow patterns in Plane C and Plane B of the IJV room are similar but not identical, not because Plane C includes the supply and the outlet but because different spreading performance of the jet in different directions. The effect of the outlet on the airflow behavior of IJV may be determined by the combination of the room height, the jet temperature and the outlet characteristics including shape, dimension and location. More work need to be done to address this issue.

Figure 9 shows the decays of dimensionless air velocity (V) along the horizontal direction (x) from the nozzle at the center line of planes of z = 0.1 m and z = 1.2 m (corresponding to the ankle and head levels for a sitting person, respectively) for different ΔT between the jet and indoor air in the case of H = 9.0 m, S =0.13 m^2, u_s = 2.0 m/s and h = 0.6 m.

The results in Figure 9 indicate that ΔT has a weak impact on the air velocity decay near the nozzle at the height of 0.1 m because the flow behavior in this region is controlled by the momentum force. When ΔT is less than 0 °C (cool jet), the airflow over the whole floor is controlled by the jet momentum. For the cases of ΔT ranging from +3 °C to +7 °C (warm jet), thermal buoyancy tends to affect the airflow pattern significantly, and the momentum-controlled area decreases with the increase of ΔT. In the zone where the jet momentum no longer dominates the airflow, air velocities at the ankle level drop quickly, but those at the head level increase sharply because of the rising plume.

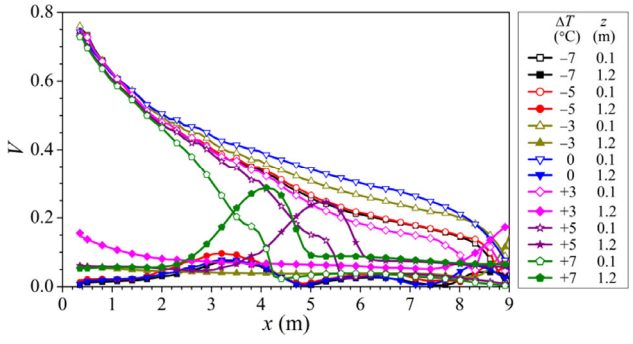

Fig. 9 Decays of dimensionless velocity (V = u/u_s) along the direction of x at the center line of two representative planes for different temperature differences

3.2 Factors affecting the flow and temperature distributions for a warm impinging jet

3.2.1 *Jet discharge height*

According to Chen et al. (2012), a smaller discharge height of an isothermal jet results in a greater air velocity and thinner airflow layer in the vicinity of the nozzle. This is attributed to the reduced air entrainment and less jet diffusion leading to more conserved momentum before the jet hits the floor. In addition, their results indicate that the differences of the magnitude of the velocity and the shape of the velocity profiles between different supply heights are decreased when moving farther from the nozzle, and all the profiles tend to coincide.

The temperature and flow fields in an IJV heating room in the case of a square grille (S = 0.13 m^2), H = 6.0 m, u_s = 1.5 m/s and ΔT = +5 °C are simulated for three nozzle heights (h), i.e., h = 0.6 m, 0.9 m and 1.2 m, to explore the impact of the discharge height of a warm jet on the airflow pattern. Figure 10 shows the air velocity and temperature profiles at the plane of z = 0.1 m for the three cases.

It can be seen from Figure 10 that when the IJV system is used for heating, both the temperature T and velocity V in the vicinity of the floor decrease with the increase of the distance from the nozzle x, and drop sharply at a certain position. The reason is that the effect of the jet's inertia relative to its buoyancy is decreased gradually during the spread of the supply jet along the floor. When the jet reaches a certain position, the inertia force is not enough to drive the supply jet forward along the floor, and finally the warm supply jet deviates from the floor and flows upward under the relatively strong effect of thermal buoyancy.

The results in Figure 10(a) show that the warm jet spreads

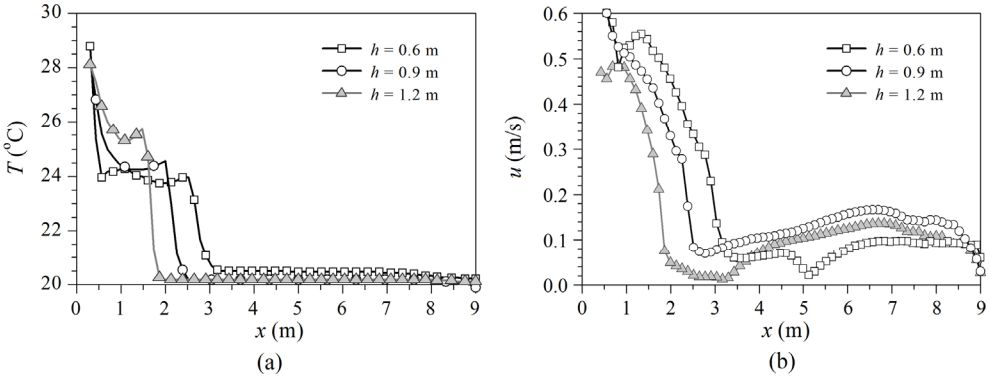

Fig. 10 Effect of jet discharge height on: (a) temperature profile and (b) velocity decay profile along the center line of the plane at z = 0.1 m

farther over the floor when the warm jet is discharged from the nozzle with a lower height. This is because the jet has more momentum after hitting the floor and the momentum-controlled region is enlarged. Figure 10(b) shows that when IJV operates in its heating mode, the maximum air velocities in the vicinity of the floor corresponding to the three discharge heights are about 0.6 m/s, 0.55 m/s and 0.5 m/s, which is an insignificant difference. It can also be observed from Figure 10(b) that the difference of the velocity decay profile along the whole floor between the three studied discharge heights is slight for the warm jet, differing from the isothermal and cool jets (Chen et al. 2012).

3.2.2 *Supply grille geometry*

Rajaratnam and Pani (1974) suggest that the decays of air velocity along the centre line of the floor for different grille shapes are almost identical for both the isothermal and cool jets. The results by Varodompun (2008) indicate that the variations of temperature along all measured angles are similar in an IJV cooling room. As for the impact of supply grille shape, some studies, such as Ren et al. (2003), Nielsen et al. (2006) and Lee et al. (2007), have discussed this topic for the cases of mixing ventilation and displacement ventilation. Varodompun (2008) investigated the impact of IJV terminal configuration in the cooling scenario and pointed out that the nozzle shape affects the airflow behavior little. However, few studies have evaluated the impact of supply grille shape of IJV when it runs in heating mode.

In the current study, the airflow fields in IJV rooms with H = 6.0 m, h = 0.6 m, u_s =1.5 m/s and ΔT = +5 °C are simulated to investigate the effect of supply grille geometry on the generated flow pattern and dispersion area of the warm jets.

The area of the supply grille is set as 0.13 m^2 firstly in this study. The results show that the grille shape affects the momentum distribution along different directions significantly after the warm jet struck the floor, but little influence is found in the cooling scenario (Varodompun 2008). The reason is that when the IJV operates in cooling mode, the buoyancy of the cool jet is downward and the confinement effect of the floor weakens its impact on airflow. In contrast, when the IJV runs in heating mode, the buoyancy of the warm jet is upward and it would not be confined by the floor.

In order to investigate the airflow features when the upward buoyancy is weakened, IJV cases with the large grille (S = 0.36 m^2) are simulated because large grille corresponds to high momentum and relatively weak buoyancy of jet. Three types of supply grille with the same area (S = 0.36 m^2), i.e., square, diamond and circular grilles (see Figure 2(d)), are taken into account, with Figure 11 presenting the air temperature distributions at the ankle level (z = 0.1 m) for the three grille geometries.

Figure 11(a) shows that the square grille tends to spread the jet equally in the longitudinal and lateral directions and to spread less air in other directions. The diamond grille appears to distribute more air in the directions perpendicular to grille surfaces and the air movement in other directions is relatively weak (Figure 11(b)). For the circular grille, see Figure 11(c), the warm air is distributed uniformly in all directions.

Figure 11 clearly shows that the influence of the supply grille geometry on the dispersion of the warm jets is different from that of the cool and isothermal jets (Rajaratnam and Pani 1974; Varodompun 2008).

3.2.3 *Ceiling height*

The air temperature fields in IJV rooms of different heights are numerically simulated for the case of u_s =1.5 m/s, h = 0.6 m, ΔT = +3 °C and S = 0.13 m^2 (square grille) for IJV operating in heating mode. Figure 12 gives the air temperature distributions and the streamlines of supply air in the vertical plane of x = 0 for four ceiling heights of 6.0, 9.0, 16.0 and 24.0 m.

It can be seen from Figure 12 that, for the ceiling heights

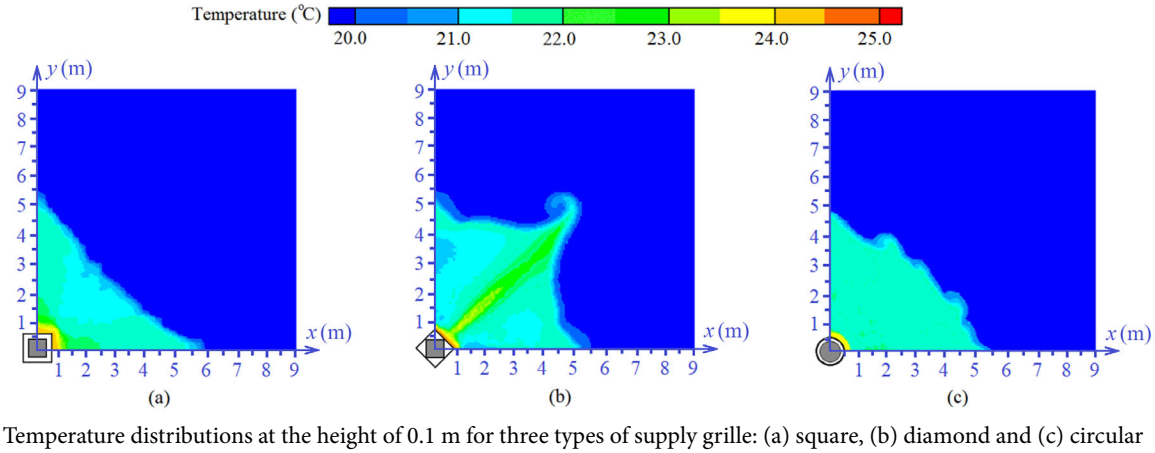

Fig. 11 Temperature distributions at the height of 0.1 m for three types of supply grille: (a) square, (b) diamond and (c) circular

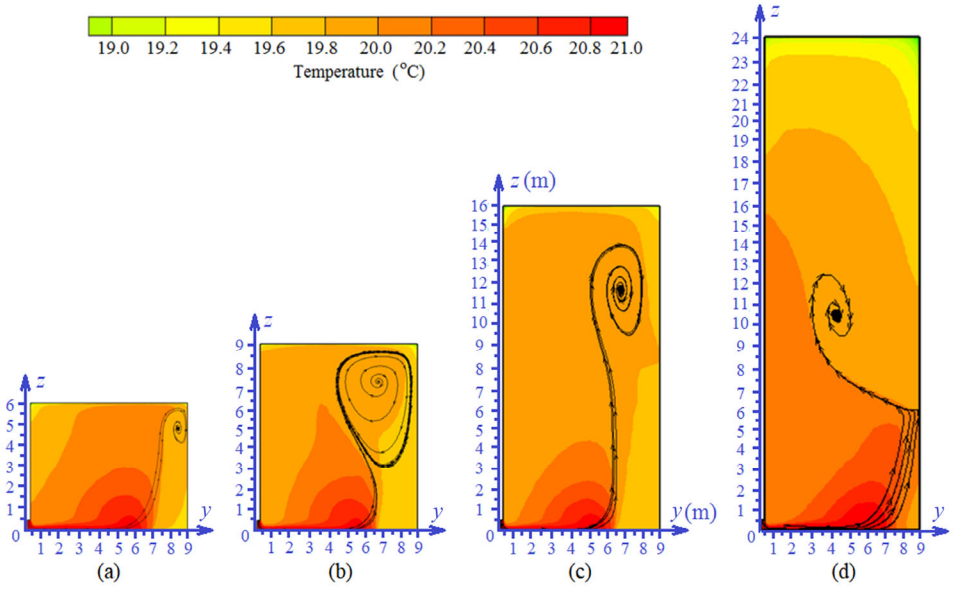

Fig. 12 Air temperature distributions and the streamlines of supply air in the vertical middle plane (x = 0) for the ceiling heights of: (a) 6.0 m, (b) 9.0 m, (c) 16.0 m and (d) 24.0 m

of 6.0 m and 9.0 m (see Figures 12(a) and (b)), the warm air goes up to the ceiling under the effect of thermal buoyancy and then forms a vortex in the vicinity of the ceiling, while for the ceiling heights of 16.0 m and 24.0 m (Figures 12(c) and (d)), the positive buoyancy is insufficient to drive the warm air to reach the ceiling, so the flow vortex is formed almost in the middle of the room height. Additionally, Figure 12 also shows that the temperature in an IJV heating room is higher in the occupied zone and is lower in the upper parts of the room for the four cases, suggesting that IJV can provide better thermal comfort and higher energy efficiency as compared to MV during the heating season, because the temperature near the floor is lower than that in the upper part for the latter (Saïd et al. 1996; Ye et al. 2016). By comparing Figures 12(a) to (d) it is speculated that the advantages of IJV relative to MV are more obvious in large-height spaces.

3.3 Analysis of draft sensation

There exists a risk of draft discomfort in the IJV room since the high momentum air is directly distributed into the occupied zone. However, only Chen et al. (2013b) investigated this problem in an IJV cooling room, and few studies refer to this for IJV in heating mode up to now.

The draught discomfort in the IJV heating room will be analyzed in this section, which is expressed as the percentage dissatisfied due to local discomfort (PD) (Fanger et al. 1988). According to ASHRAE standard 55 (ASHRAE 2010), the maximum allowable value for PD is 20%. Since the ankle is the most sensitive part of body due to draught because of less clothing insulation and higher air velocity near the floor than other regions in IJV rooms, the PD is assessed at the ankle level, i.e., 0.1 m above the floor. PD is determined by Fanger's equation (Fanger et al. 1988), which is written as:

$$\mathrm{PD} = (T_{\mathrm{cl}} - T)(\overline{u} - 0.05)^{0.62}(3.14 + 0.37\overline{u}T_{\mathrm{u}}) \tag{9}$$

(when $\overline{u}$ < 0.05 m/s, use $\overline{u}$ = 0.05 m/s; for PD > 100%, use PD = 100%)

where $\overline{u}$ is the mean velocity, T is the air temperature, T_{cl} is the mean skin temperature. T_{cl} is usually set to be 34 °C for the bare skin including bare ankle. However, the ankle is usually covered with socks in winter and the temperature of the sock surface is lower than that of the bare skin, so PD might be overestimated. The expression of $T_{\mathrm{cl}} = T$ + (5 to 7 °C) for an ankle covered with socks is proposed to estimate the value of PD more reliably in an IJV heating room.

By collecting the numerical results, the PD is calculated for the case of ΔT = + 3 °C, H = 9.0 m, h = 0.6 m and square grille (S = 0.13 m^2) with three different supply velocities, with Figure 13 giving the distribution of PD at the plane of z = 0.1 m for u_{s} = 1.0 m/s and 2.0 m/s. It can be known from Figure 13 that even though the air temperature near the floor is high (see Figure 11) the value of PD in this region is large because the velocity is higher in this region than in other regions of the IJV room.

Figure 14 shows the relationship between the maximum PD ($\mathrm{PD}_{\mathrm{max}}$) and supply velocity ($u_{\mathrm{s}}$). The effect of ankle surface temperature (34 °C for bare ankle and 27 °C for dressed ankle) on the value of $\mathrm{PD}_{\mathrm{max}}$ has also been evaluated.

It can be found in Figure 14 that $\mathrm{PD}_{\mathrm{max}}$ increases with the

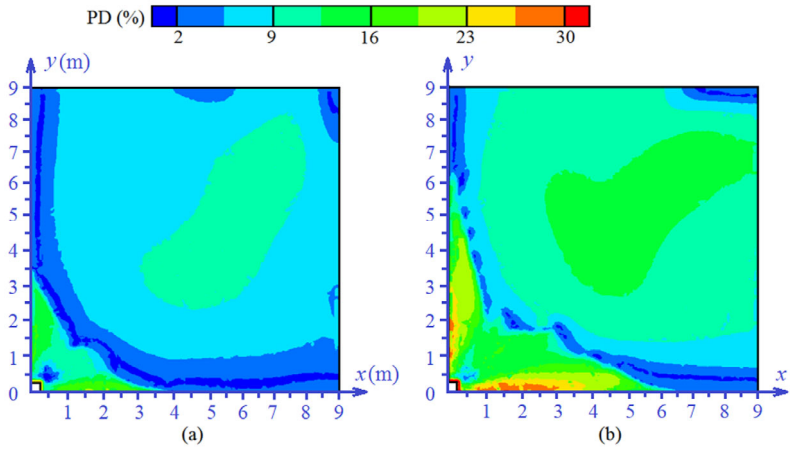

Fig. 13 Predicted PD distribution at the ankle level (z = 0.1 m) for: (a) u_s =1.0 m/s and (b) u_s =2.0 m/s

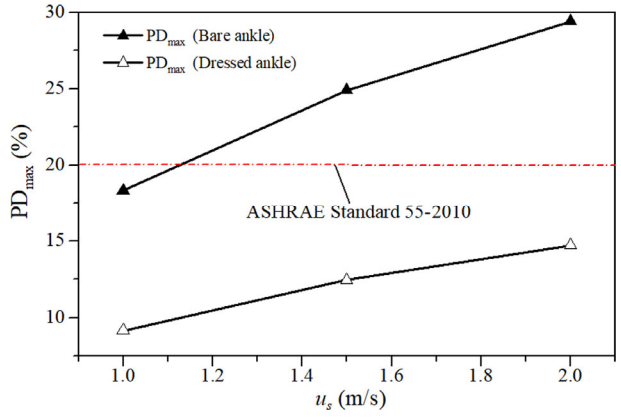

Fig. 14 Effects of supply velocity u_s on the maximum PD (PD_{max})

increase of supply velocity. For dressed ankle, the values of PD_{max} are all smaller than 20% for the three supply velocities studied. While the value of PD_{max} for the case of u_s being 2.0 m/s is up to 29% for bare ankle, which is much greater than the allowable value (20%). Consequently, it is recommended to wear socks in order to avoid thermal discomfort in an IJV heating room.

4 Conclusion

Numerical simulations are carried out to investigate the airflow and temperature fields in an IJV room with cool, isothermal or warm jets. Influences of jet discharge height, supply grille shape and room height on the airflow behavior are analyzed by using numerical results. Furthermore, the influence of supply velocity on the draught discomfort is discussed in detail when IJV runs in its heating mode.

The numerical results indicate that the supply air always spreads along the whole floor when IJV is operated in cooling or isothermal scenarios, while the flow pattern of the warm jet differs from that of the cool or isothermal jets, since the thermal buoyancy of the warm air is acting in the opposite direction. The warm supply air separates from the floor and flows upwards to the ceiling after it spreads a certain distance due to the thermal buoyancy effect, which results in limited air dispersion area over the floor. The larger the temperature difference of the supply air, the smaller the dispersion area.

For a heating room equipped with IJV, the influences of the jet discharge height, the shape of supply inlet and the ceiling height on the air temperature and velocity profiles in the room are significantly different from those of the cool and isothermal jets. If the warm jet is discharged from the nozzle with a lower height, it would spread farther over the floor, while the supply grille shape and ceiling height almost have no effect on the warm air dispersion area. The results also indicate that the temperature in the rest of the IJV heating room is almost the same, except that the temperature near the floor is slightly higher within the zone of warm jet flow, which is different from that in a MV heating room where the indoor air temperature is lower in the occupied zone and is higher in the upper zone. This means that the IJV system has obvious advantages over the MV system in ensuring the thermal comfort in the occupied zone and improving energy efficiency, and the higher the room height is, the more obvious the advantage of IJV over MV.

Moreover, the draught discomfort analysis shows that the value of PD near the floor might be greater than the acceptable range specified by ASHRAE standard when the ankle is bare, since the velocity in the region near the floor is high in the IJV room. It is recommended to wear socks to avoid thermal discomfort caused by IJV.

Acknowledgements

This work was supported by the National Natural Science Foundation of China (No. 51278094 and No. 51478098),

the Innovation Foundation of Shanghai Education Commission (No. 13ZZ054) and the Natural Science Foundation of Jiangsu Province, China (No. BK20161336).

References

ASHRAE (2010). ASHRAE Standard 55: Thermal Environmental Conditions for Human Occupancy. Atlanta: American Society of Heating, Refrigerating and Air-Conditioning Engineers.

Awbi HB (2003). Ventilation of Buildings, 2nd edn. London: Taylor and Francis.

Beltaos S, Rajaratnam N (1973). Plane turbulent impinging jets. *Journal of Hydraulic Research*, 11: 29–59.

Beltaos S, Rajaratnam N (1974). Impinging circular turbulent jets. *Journal of the Hydraulics Division*, 100: 1313–1328.

Beltaos S, Rajaratnam N (1977). Impingement of axisymmetric developing jets. *Journal of Hydraulic Research*, 15: 311–326.

Chen Q (1995). Comparison of different *k*-ε models for indoor air flow computations. *Numerical Heat Transfer, Part B: Fundamentals*, 28: 353–369.

Chen HJ, Moshfegh B, Cehlin M (2012). Numerical investigation of the flow behavior of an isothermal impinging jet in a room. *Building and Environment*, 49: 154–166.

Chen HJ, Moshfegh B, Cehlin M (2013a). Investigation on the flow and thermal behavior of impinging jet ventilation systems in an office with different heat loads. *Building and Environment*, 59: 127–144.

Chen H, Moshfegh B, Cehlin M (2013b). Computational investigation on the factors influencing thermal comfort for impinging jet ventilation. *Building and Environment*, 66: 29–41.

Chen H (2014). Experimental and numerical investigations of a ventilation strategy—Impinging jet ventilation for an office environment. PhD Thesis, Linköping University, Sweden.

Chen H, Janbakhsh S, Larsson U, Moshfegh B (2015). Numerical investigation of ventilation performance of different air supply devices in an office environment. *Building and Environment*, 90: 37–50.

Cooper D, Jackson DC, Launder BE, Liao GX (1993). Impinging jet studies for turbulence model assessment—I. Flow-field experiments. *International Journal of Heat and Mass Transfer*, 36: 2675–2684.

Fanger PO, Melikov AK, Hanzawa H, Ring J (1988). Air turbulence and sensation of draught. *Energy and Buildings*, 12: 21–39.

Gauntner JW, Livingood JNB, Hrycak P (1970). Survey of literature on flow characteristics of a single turbulent jet impinging on a flat plate. NASA Technical Note (NASA TN D-5652).

Guerra DRS, Su J, Silva Freire AP (2005). The near wall behavior of an impinging jet. *International Journal of Heat and Mass Transfer*, 48: 2829–2840.

Gutmark E, Wolfshtein M, Wygnanski I (1978). The plane turbulent impinging jet. *Journal of Fluid Mechanics*, 88: 737–756.

Haghshenaskashani S, Sajadi B, Cehlin M (2018). Multi-objective optimization of impinging jet ventilation systems: Taguchi-based CFD method. *Building Simulation*, 11: 1207–1214.

Karimipanah T, Awbi HB (2002). Theoretical and experimental investigation of impinging jet ventilation and comparison with wall displacement ventilation. *Building and Environment*, 37: 1329–1342.

Kim K-S (1993). An experimental study on the flow and heat transfer characteristics of an impinging jet. *KSME Journal*, 7: 258–271.

Knowles K, Myszko M (1998). Turbulence measurements in radial wall-jets. *Experimental Thermal and Fluid Science*, 17: 71–78.

Launder BE, Spalding DB (1974). The numerical computation of turbulent flows. *Computer Methods in Applied Mechanics and Engineering*, 3: 269–289.

Lee E, Khan JA, Feigley CE, Ahmed MR, Hussey JR (2007). An investigation of air inlet types in mixing ventilation. *Building and Environment*, 42: 1089–1098.

Nielsen PV, Heby T, Moeller-Jensen B (2006). Air distribution in a room with ceiling-mounted diffusers—Comparison with wall-mounted diffuser, vertical ventilation, and displacement ventilation. *ASHRAE Transactions*, 112(2): 498–504.

Rajaratnam N, Pani BS (1974). Three-dimensional turbulent wall jets. *Journal of the Hydraulics Division*, 100: 69–83.

Ren H, Zhao B, Li X, Fan H, Yang X (2003). Influence of diffuser jet characteristics on indoor air distribution under actual connecting conditions. *Journal of Architectural Engineering*, 9: 141–144.

Saïd MNA, MacDonald RA, Durrant GC (1996). Measurement of thermal stratification in large single-cell buildings. *Energy and Buildings*, 24: 105–115.

Taghinia J, Rahman M, Siikonen T (2015). Simulation of indoor airflow with RAST and SST-SAS models: A comparative study. *Building Simulation*, 8: 297–306.

Varodompun J (2008). Architectural and HVAC applications of impinging jet ventilation using full scale and CFD simulation. PhD Dissertation, University of Michigan, USA.

Xu Z, Hangan H (2008). Scale, boundary and inlet condition effects on impinging jets. *Journal of Wind Engineering and Industrial Aerodynamics*, 96: 2383–2402.

Yao S, Guo Y, Jiang N, Liu J (2015). Experimental investigation of the flow behavior of an isothermal impinging jet in a closed cabin. *Building and Environment*, 84: 238–250.

Ye X, Zhu H, Kang Y, Zhong K (2016). Heating energy consumption of impinging jet ventilation and mixing ventilation in large-height spaces: A comparison study. *Energy and Buildings*, 130: 697–708.

Ye X, Kang Y, Zuo B, Zhong K (2017). Study of factors affecting warm air spreading distance in impinging jet ventilation rooms using multiple regression analysis. *Building and Environment*, 120: 1–12.

Ye X, Kang Y, Yang X, Zhong K (2018). Temperature distribution and energy consumption in impinging jet and mixing ventilation heating rooms with intermittent cold outside air invasion. *Energy and Buildings*, 158: 1510–1522.

Zhao W, Kumar K, Mujumdar AS (2004). Flow and heat transfer characteristics of confined noncircular turbulent impinging jets. *Drying Technology*, 22: 2027–2049.

Zuo B, Zhong K, Kang Y (2015). An experimental study on particle resuspension in a room with impinging jet ventilation. *Building and Environment*, 89: 48–58.